



Fast Gated Superconducting Nanowire Camera for Multi-Functional Optical Tomograph

Grant Agreement Nº 101099291

WP 4

D4.2: Laser configuration

Lead Beneficiary: Politecnico di Milano (CUSBO)

Due date of deliverable: 31.03.2025

Type and dissemination level: Document, Public



Table of Contents

About fastMOT	1
Executive summary	2
Abbreviations	3
List of contributors	4
1 Introduction and objectives	5
2 Definition of first laser for TD-DCS	5
2.1 Problem	5
2.2 Setup	5
2.3 Analysis	7
2.4 Results	g
3 Definition of second laser for TD-NIRS	14
3.1 Problem	14
3.2 Setup	15
3.3 Analysis	16
3.4 Results	17
4 Conclusion	22
5 References	23

List of figures

Figure 1: The measured value of αDb for a static liquid phantom made of water and intralipid. It's over 100 seconds for the 6 combinations of parameters shown. The green horizontal line represents the mean value of αDb while the horizontal dashed line represents +/- 10% variations from the mean. The measurement shows that the measured value of αDb is quite stable over several combinations.

Figure 2: Left: the measured value of β against the pulse duration setting of the laser. Right: the stability error for the plots against the pulse duration setting of the laser. Each plot has 4 curves representing 2 different repetition rates (100MHz and 10MHz) and for 2 different types of time gating: same time gate duration as pulse duration (TD) and 3000 ps long time gate (quasi-CW).



Figure 3: Horizontality of the measured value of α Db against pulse duration of the laser. Horizontality is calculated here as the slope of the linear fit of the data, multiplied by 100 s and divided by the mean value of α Db. The plot has 4 curves representing 2 different repetition rates (100 MHz and 10 MHz) and for 2 different types of time gating: same time gate duration as pulse duration (TD) and 3000 ps long time gate (quasi-CW).
Figure 4: Results of time-gated analysis of DCS data. Two laser repetition rates were measured with slightly different IRF widths (subplot A). In subplots B and C, a zoom-in of the IRF together with the respective measured DTOFs are shown for the measurement at 10 MHz (subplot B) and the measurement at 100 MHz (subplot C). Values of β (subplot E) were estimated from the time-gated g_2 curves (subplot D). Using these values of β , g_1 was calculated and finally αD_b was derived for all of the time-gates that were considered (subplot F). The time-gates were chosen so that their widths were approximately equal to the FWHM of the IRF, and each time-gate overlapped with 80% of the previous time-gate. The shaded regions in subplot B and C indicate the limits of the time gates which displayed relatively stable values of αD_b . The dashed vertical line in subplots B and C indicate the upper limit of the last considered time gate
Figure 5: The measured value of αDb for liquid phantoms with varying concentrations of glycerol (as percentage of mass), but constant optical properties, plotted over the theoretical expectation based on experimental values of viscosity for water-glycerol mixtures and a theoretical model relating the viscosity of a liquid to its Db coefficient. This measurement was done with the laser set at 100 MHz and 300 ps pulse duration.
Figure 6: Relative change of the Db coefficient with respect to the baseline value for a task including: 350 s of rest, 300 s of arterial occlusion and 250 s of recovery. This measurement was done with the laser at 100 MHz and 300 ps pulse duration
Figure 7: Relative change of the Db coefficient with respect to the baseline value for a task including: 350 s of rest, 300 s of arterial occlusion and 250 s of recovery. This measurement was done with the laser at 100 MHz and 300 ps pulse duration
Figure 8: Left: the condition number of the matrix of specific absorptions plotted against the wavelength coupled to 1064 nm and Right: the percentage uncertainty of the measured baseline values of the total haemoglobin concentration (averaged over the three volunteers) plotted against the wavelength coupled to 1064 nm

Figure 9: Haemoglobin related quantities evaluated at each second wavelength (the wavelength



Figure 10: The error (on haemoglobin related quantities) associated to the uncertainty in the water absorption of the biological sample analysed. This error is evaluated for four quantities, going from top left to bottom right: concentration of Hb, concentration of HbO2, saturation of the blood, total haemoglobin concentration. The errors are plotted against the second wavelength (the wavelength coupled to 1064 nm).

Disclaimer

This document is part of the deliverables from the project fastMOT, which has received funding from the European Union. Views and opinions expressed are however those of the author(s) only and do not necessarily reflect those of the European Union or the European Commission. Neither the European Union nor the granting authority can be held responsible for them.



About fastMOT

Traditionally, the monitoring of organs and deep body functional imaging is done by ultrasound, X-Rays (incl. CT), PET or MRI. These techniques only allow for very limited measurements of functionality, usually combined with exogenous and radioactive agents. In this project we are developing an innovative light sensing solution, a fast gated, ultra-high quantum efficiency single-photon sensor, to enable multi-functional deep body imaging with diffuse optics.

The new type of sensor is based on superconducting nanowire single-photon detectors that have shown to be ultra-fast and highly efficient. However, until now the active area and number of pixels has been limited to micrometres diameter and tens of pixels. We are using a combination of new techniques to overcome this limit and scale to 10,000 pixels and millimetre diameter.

In addition, we are developing new strategies for performing TD-NIRS and TD-SCOS to use this new light sensor optimally with Monte-Carlo simulations. We will implement the new light sensor in an optical tomograph and achieve a 100x improvement of SNR compared to using existing light sensors. With our Multifunctional Optical Tomograph we will be able to image deep organ and optical structures and monitor functions including oxygenation, haemodynamics, perfusion and metabolism.



Executive summary

In this deliverable we present the effect of key laser parameters (e.g., optimal pulse width and wavelength) on TD-SCOS (Time Domain Speckle Contrast Optical Spectroscopy) and TD-NIRS (Time Domain Near Infrared Spectroscopy), permitting the identification of the best feasible laser configuration for the fastMOT prototype, thus leading to a suitable laser source choice. This is also the outcome of task T4.2 "Laser sources for TD-SCOS and TD-NIRS".

For TD-SCOS/TD-DCS (Time Domain Diffuse Correlation Spectroscopy) a suitable laser with high temporal coherence yet pulsed (hundreds of ps) operation is needed. The laser technology that we identified is based on a highly temporally coherent CW source with a fast modulator to slice laser pulses, followed by a laser amplifier. We opted to operate at 1064 nm, exploiting the key advantages of long wavelengths for DCS/SCOS (e.g. lower scattering, higher number of photons for the same average power, longer decorrelation time, ...). The high quantum efficiency of the SNSPD even in the NIR region entitled us to operate in this interesting spectral range – still largely unexplored because of limitations of standard single-photon detectors (e.g. silicon SPADs).

On the other side, the laser source for TD-NIRS is less demanding, since pulsed but not extremely narrowband sources are required. Yet, to quantify both Hb (deoxyhaemoglobin) and HbO₂ (oxyhaemoglobin), leading to total haemoglobin content and tissue oxygenation, at least two wavelengths are needed.

For what concerns the TD-DCS/TD-SCOS source, we studied the repetition rate and pulse width to determine the best operative conditions of the laser, while for TD-NIRS the couple of wavelengths to retrieve of HbO₂ and Hb was investigated.

We investigated both problems using two laser sources:

- a single wavelength (1064 nm) laser with variable pulse width and repetition rate based on the technology described above (Manny laser, Irisiome Solutions, France);
- a supercontinuum 40 MHz pulsed laser equipped with an acousto-optic filter for fast selection of up to 8 wavelengths (SuperK FIANIUM, NKT Photonics, Denmark).

Using the 1064 nm laser, we studied the effect of repetition rate and pulse width duration on TD-DCS acquisition. More in detail, we evaluated the stability of the D_b coefficient for a liquid phantom with constant viscosity – prepared using the instructions found in [1] – and the evolution of D_b with a changing viscosity of the liquid phantom. We also carried out an in-vivo cuff occlusion measurement to validate the parameter choice. The suitability of 1064 nm to retrieve the concentration of HbO₂



[2], thus granting its use for the fastMOT project.

To identify the second laser wavelength, measurements at eight candidate wavelengths simultaneously were done using the supercontinuum laser. A task composed of two cuff occlusions (i.e., an arterial and a venous one) was performed on 3 healthy subjects. The analysis demonstrated the capability of the 1064 nm wavelength coupled with a second source <800 nm to track temporal changes in Hb and HbO₂, whereas the absolute values at baseline are partially affected by the estimate of water content.

Abbreviations

Abbreviation	Definition
BFI	Blood Flow Index
CW	Continuous Wave
CW-DCS	Continuous Wave Diffuse Correlation Spectroscopy
DCS	Diffuse Correlation Spectroscopy
DTOF	Distribution of Times Of Flight
FWHM	Full Width Half-Maximum
GPIO	General Purpose Input/Output
Hb	Deoxyhaemoglobin
HbO ₂	Oxyhaemoglobin
IRF	Instrument Response Function
NIRS	Near Infrared Spectroscopy
SNSPD	Superconducting Nanowire Single-Photon
TD-DCS	Time Domain Diffuse Correlation Spectroscopy
TD-NIRS	Time-Domain Near Infrared Spectroscopy
TD-SCOS	Time domain speckle contrast optical spectroscopy
WP	Work Package



List of contributors

Institution	Name
CUSBO	Tommaso Palo <tommaso.palo@polimi.it></tommaso.palo@polimi.it>
CUSBO	Laura Di Sieno <laura.disieno@polimi.it></laura.disieno@polimi.it>
CUSBO	Antonio Pifferi <antonio.piferri@polimi.it></antonio.piferri@polimi.it>
CUSBO	Alberto Dalla Mora <alberto.dallamora@polimi.it></alberto.dallamora@polimi.it>
ICFO	Lisa Kobayashi Frisk <lisa.kobayashi@icfo.eu></lisa.kobayashi@icfo.eu>
ICFO	Turgut Durduran <turgut.durduran@icfo.eu></turgut.durduran@icfo.eu>



1 Introduction and objectives

The objective of this deliverable is to identify the best feasible laser source configuration for the fastMOT prototype. To this end, we evaluated the compatibility of a 1064 nm laser with TD-DCS across its parameter space by studying the precision of its measurement outcome when analysing a liquid phantom. We then changed the viscosity of the liquid phantom and evaluated the accuracy of the measurement outcome by comparing it with the theoretically expected change. Finally, the laser source was used at a suitable parameter configuration for an in-vivo cuff occlusion measure to validate the laser and the settings used.

For TD-NIRS it was essential to evaluate the best combination of wavelengths to extract the concentrations of HbO_2 and Hb from the measurements. We investigated the possibility of using 1064 nm coupled to a second wavelength to carry out TD-NIRS For that purpose, we carried out three cuff occlusions on three healthy volunteers.

2 Definition of first laser for TD-DCS

2.1 Problem

While we based the initial work for WP 4 on the active mode-locked Titanium-Sapphire laser source available at CUSBO, it is not a suitable source for the final prototype due to its delicate alignment procedure and relative instability. An alternative, more stable and compact, laser source was investigated: a 1064 nm pulsed laser with variable pulse duration and repetition rate. Due to their impact on the measurement outcomes for TD-DCS/SCOS, its parameter combinations were analysed to determine a good operating configuration.

To define the first laser source for TD-DCS we carried out three different experiments. Firstly, a number of different parameter combinations was investigated against the measured relative Brownian motion coefficient (αD_b) over 10 minutes. Secondly, a good parameter combination was selected from the first experiment to study a set of phantoms with increasing viscosity and compare the evolution of the coefficient against the theoretical expectation. Thirdly, the same parameter combination was used for an in-vivo cuff-occlusion measurement to validate the laser configuration.

2.2 Setup

The 1064 nm laser (Manny laser, Irisiome Solutions, France) requires an input clock from an external source, which we provided through a custom-made pulse generator. The output of this pulse generator was split in two as to provide a synchronisation signal to the time tagger (Time Tagger X,



Swabian Instruments, Germany). The light coming out of the laser was transported with a 50 μ m core fibre to a collimator, which was directed with free space propagation towards a variable optical attenuator (used to adjust the intensity of the beam at the injection fibre), after which the light entered another collimator that collected the light inside another 50 μ m core fibre. This is the injection fibre with NA of 0.2. For IRF measurements, light would then pass through a thin layer of Teflon to scramble the direction vectors of light and then enter the detection fibre with a 5 μ m core and NA of 0.13. For non-IRF measurements instead, the detection fibre was held 1.5 cm away from the injection fibre with a small 3-D printed probe. This fibre was connected to an SNSPD detector tuned for 1064 nm light (Single Quantum, the Netherlands). The electrical signal coming out of the detector was directed to the time tagger, the time tags data produced by it was then passed onto a computer for analysis through USB connection.

For the first experiment we analysed a liquid phantom with an absorption coefficient of 0.0144 mm^{-1} and a reduced scattering coefficient of 0.4523 mm^{-1} at 1064 nm (700.24 g of water and 23.74 g of Intralipid 20%) [1]. The 1064 nm laser was first set to a pulse repetition rate of 100 MHz and then to 10 MHz. The pulse duration was varied automatically with a stepper motor from 500 ps to 100 ps with steps of 100 ps. The laser stayed at a specific parameter combination for 10 minutes.

For the second experiment we analysed a liquid phantom firstly composed of 500 g of water, 26 g of Intralipid 20% and 1.2 g of black ink (9.14 \times 10⁻³ dilution). After each measurement we increased the mass concentration of glycerol by steps of 10% [1] until we reached a phantom made of 30% glycerol:

- 10% concentration: We added 59.2 g of glycerol and 6.93 g of Intralipid 20%
- 20% concentration: We added 76.8 g of glycerol and 11.34 g of Intralipid 20%
- 30% concentration: We added 104.6 g of glycerol and 17.4 g of Intralipid 20%

Intralipid 20% was progressively added to keep the optical properties of the phantom constant throughout the experiment. The 1064 nm laser was configured to have a pulse duration of 300 ps and repetition rate of 100 MHz throughout the whole experiment. The rest of the optical setup and detection setup remained unchanged from the first experiment. Each measurement lasted 3 minutes.

For the third experiment we carried out a cuff-occlusion experiment on a healthy volunteer.

We followed the task below:

- 350 seconds of rest (baseline),
- 300 seconds of arterial occlusion at 200 mm Hg,



250 seconds of recovery.

The 1064 nm laser was configured to have a pulse duration of 300 ps and repetition rate of 100 MHz throughout the whole experiment. The rest of the optical setup and detection setup remained unchanged from the first experiment. The fibres were placed facing the skin of the healthy volunteer on the inside part of the right forearm on the most muscular area. They were held still by a probe with source-detector separation of 1.5 cm and the probe was wrapped around their arm with medical tape.

For the task-related setup, we wrapped a blood pressure cuff around the right bicep of the volunteer and inflated it manually following the task described above.

2.3 Analysis

The data from these measurements comes in time tags, which means the absolute arrival time of each photon recorded with an accuracy of a few picoseconds. From the macro-time of arrival of the photons one can extract roughly the intensity of light at the detection fibre over time. The intensity depends on the flickering of the speckle pattern, which is formed due to the random phase shifts induced by the scattering events inside the optical medium. When the scatterers are moving, the flickering of the speckle pattern can be related to the movement of the scatterers. This forms the basis of DCS and SCOS.

In DCS, the intensity autocorrelation of the speckle pattern $g_2(\tau)$ is measured. From $g_2(\tau)$, the electric-field autocorrelation function $g_1(\tau)$ can be derived using the Siegert relation:

$$g_2(\tau) = 1 + \beta |g_1(\tau)|^2$$
 (eq. 1)

Where in eq. 1 β is a coefficient which depends on the properties of the system such as the coherence of the laser source and the detected polarization. $g_1(\tau)$ can be shown to have the following form when measuring in a reflection geometry [3]:

$$g_1(\tau) = \frac{1}{G_1(0)} \left(\frac{e^{-r_1 K(\alpha D_b \tau)}}{r_1} - \frac{e^{-r_b K(\alpha D_b \tau)}}{r_b} \right)$$
 (eq. 2)

where $G_1(0)$, r_1 and r_b are constants that depend on the optical properties of the system as well as the source-detector separation and the laser wavelength, $K(\alpha Db\tau)$ is a term that depends on $\alpha D_b\tau$ and on the system optical properties as well as the laser wavelength. One can recover $\alpha D_b\tau$ using minimization algorithms to fit the experimental data to theory [3] [4].

Time domain DCS (TD-DCS) was also implemented in the analysis of the some of the data in this deliverable. In comparison to CW-DCS, in TD-DCS $g_1(\tau)$ curves are computed with photons that



were detected within a defined range of micro-times (i.e. time-gate) in the order of magnitude of the DTOF (Distribution of Times of Flight) width. αD_b can be extracted from the time-gated $g_1(\tau)$ curves in a similar manner to CW-DCS however, corrections must also be applied to correct for IRF effects [3]

For the first experiment the data was analysed using TD-DCS. In this case for a pulse duration setting of X ps, the time-gate to filter the photons was selected to start from the peak of the DTOF and last for X ps. This was done to improve the correlation of the analysed light since closer times in the DTOF correlates to closer real times of flight, that correlates to similar spatial paths in the biological sample and hence interaction with the same scatterers. The time-gated analysis was also carried out to evaluate the ability of the laser to operate in TD-DCS, since a continuous wave analysis would only confirm its operation in DCS. Time gating is essential for depth selectivity.

In this analysis we used an integration time of 1 second and analysed the first 100 seconds. Each integration represented one value of rD_b for statistical studies and graphical representation, leading to a total of 100 values. For each parameter combination we extracted a mean value of rD_b , its standard deviation and then obtained a percentage error ($\%err = \frac{std(rD_b)}{mean(rD_b)}$).

We also conducted a quasi-CW analysis of the same data by inserting time gates that begin 500 ps before the peak of the DTOF and last for 3 ns (which is substantially wider than the IRF). This was done for each parameter combination to compare the β values and the percentage error. Further, we carried out a linear fit of the rD_b values against time for the TD and quasi-CW analysis to verify the linear trend of the data, which was expected to have a gradient of zero.

A further analysis was carried out to study the impact of time gate positioning specifically for the laser settings of 100 MHz, 300 ps and 10 MHz, 500 ps. By applying time gates of duration equal to the pulse duration, and setting start several times such that successive gates overlap by 80 % until the entire measured DTOF is incorporated, a total of 27 time-gates (100 MHz data) and 30 time-gates (10 MHz data) were considered. For each time-gate, the coherence coefficient β was derived and subsequently g_1 was obtained. Finally, we derived values of αD_b by fitting g_1 using the correction algorithm detailed in [3]. All the results are reported in section 2.4.

For the second experiment the data was analysed CW-DCS (Continuous Wave DCS). The ability of the system to operate under time-gates had already been verified in the previous experiment, and both accuracy and in-vivo validation can be carried out with a continuous analysis. The integration time in this case was 20 seconds, yielding rD_b values from which to evaluate a mean and a standard deviation for each glycerol concentration percentage. To obtain an absolute value



for D_b we used the following equation:

$$rac{rD_b(a\%)}{rD_b(b\%)} = rac{\eta(b\%)}{\eta(a\%)}$$
 (eq.

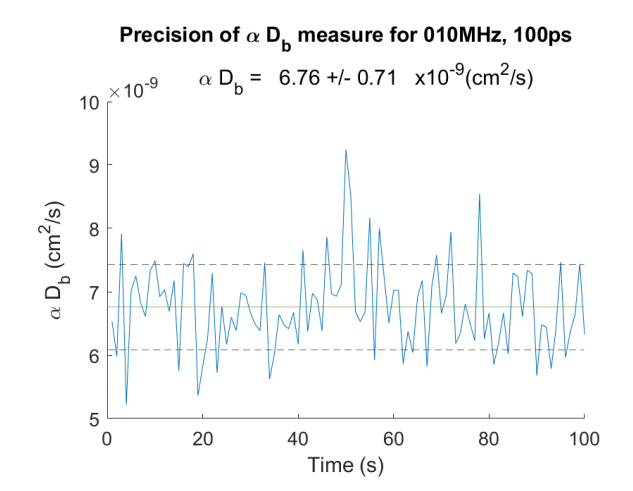
3)

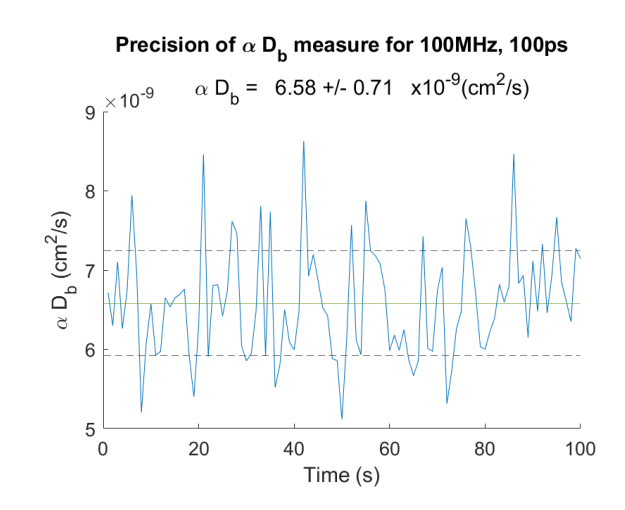
where $D_b(a\%)$ is the relative value of D_b for a glycerol mass concentration of a% and η is the viscosity coefficient [4]. From this equation we assumed that one of the data points was correct (the choice was done based on the uncertainty of each point) and then proceeded to plot the theoretical expectation based on the known values of the viscosity coefficient η [5] for glycerol concentrations up to 30%.

For the third experiment, the data was analysed using CW-DCS. The 15-minute-long measurement was split into 900 sections each lasting 1 second and resulting in a value for rD_b . Each resulting value of rD_b was then plotted against time.

2.4 Results

For the first part of the experiment, a liquid phantom at rest was observed. Below, we display examples of the measured αD_b for four parameter combinations.







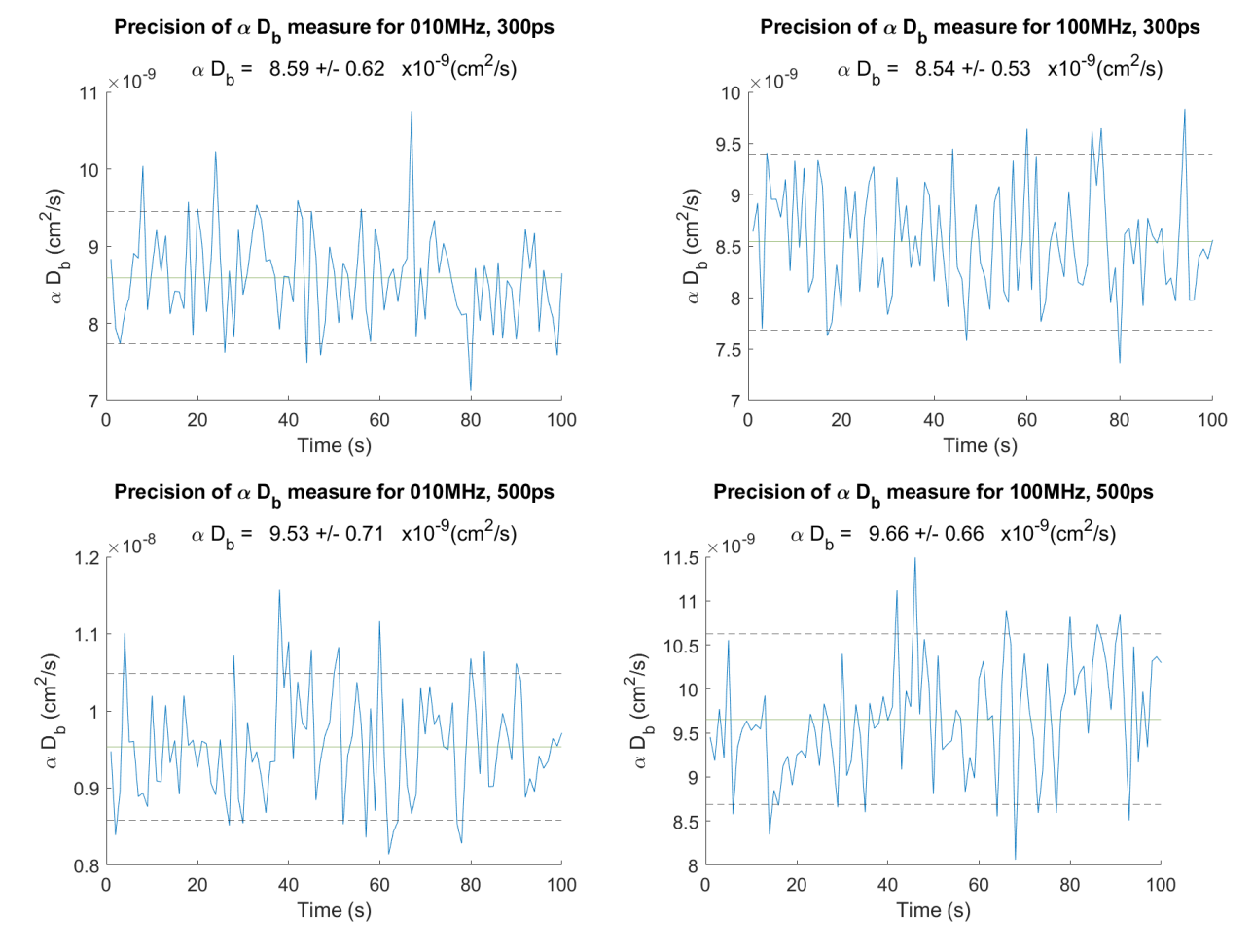


Figure 1. The measured value of αDb for a static liquid phantom made of water and intralipid. It's over 100 seconds for the 6 combinations of parameters shown. The green horizontal line represents the mean value of αDb while the horizontal dashed line represents +/- 10% variations from the mean. The measurement shows that the measured value of αDb is quite stable over several combinations.

As can be seen in Figure 1, each parameter combination has a different level of noise or instability associated with this static measure. The values of these errors and the mean β value for each parameter combination are shown in the plots below.



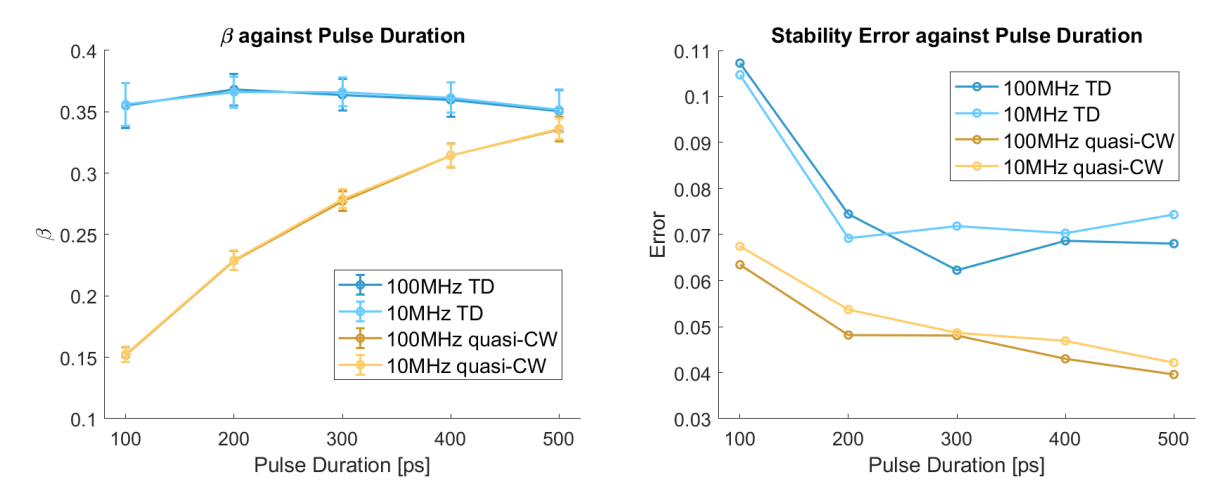


Figure 2. Left: the measured value of β against the pulse duration setting of the laser. Right: the stability error for the plots against the pulse duration setting of the laser. Each plot has 4 curves representing 2 different repetition rates (100MHz and 10MHz) and for 2 different types of time gating: same time gate duration as pulse duration (TD) and 3000 ps long time gate (quasi-CW).

As can be seen in Figure 2, the β value remains high and roughly constant for time gates with size equal to the pulse duration setting. For a large constant time gate (CW) the β value increases with the pulse duration as should be expected. Another interesting thing to note is the similarity for the plots at 100 MHz and 10 MHz, showing that the 1064 nm laser operates similarly at these repetition rates. The stability error is low throughout the parameter space thus allowing us to conclude that there is a range of values that are suitable for TD-DCS experiments. Also, as can be seen in the plot below, the measured αD_b shows no trend, increasing or decreasing, as should be expected.

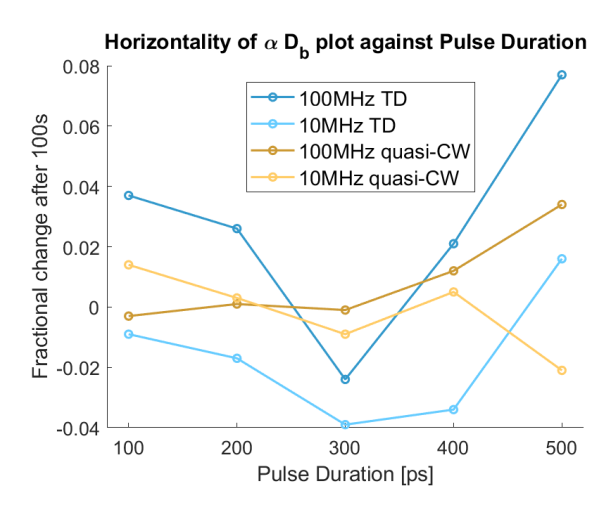


Figure 3. Horizontality of the measured value of α Db against pulse duration of the laser. Horizontality is calculated here as the slope of the linear fit of the data, multiplied by 100 s and divided by the mean value of α Db. The plot has 4 curves representing 2 different repetition rates (100 MHz and 10 MHz) and for 2 different types of time gating: same time gate duration as pulse duration (TD) and 3000 ps long time gate (quasi-CW).



For the final analysis of the first part of the experiment, the dependence of β and αD_b on the position of the time gates was studied, as can be seen in the plots below.

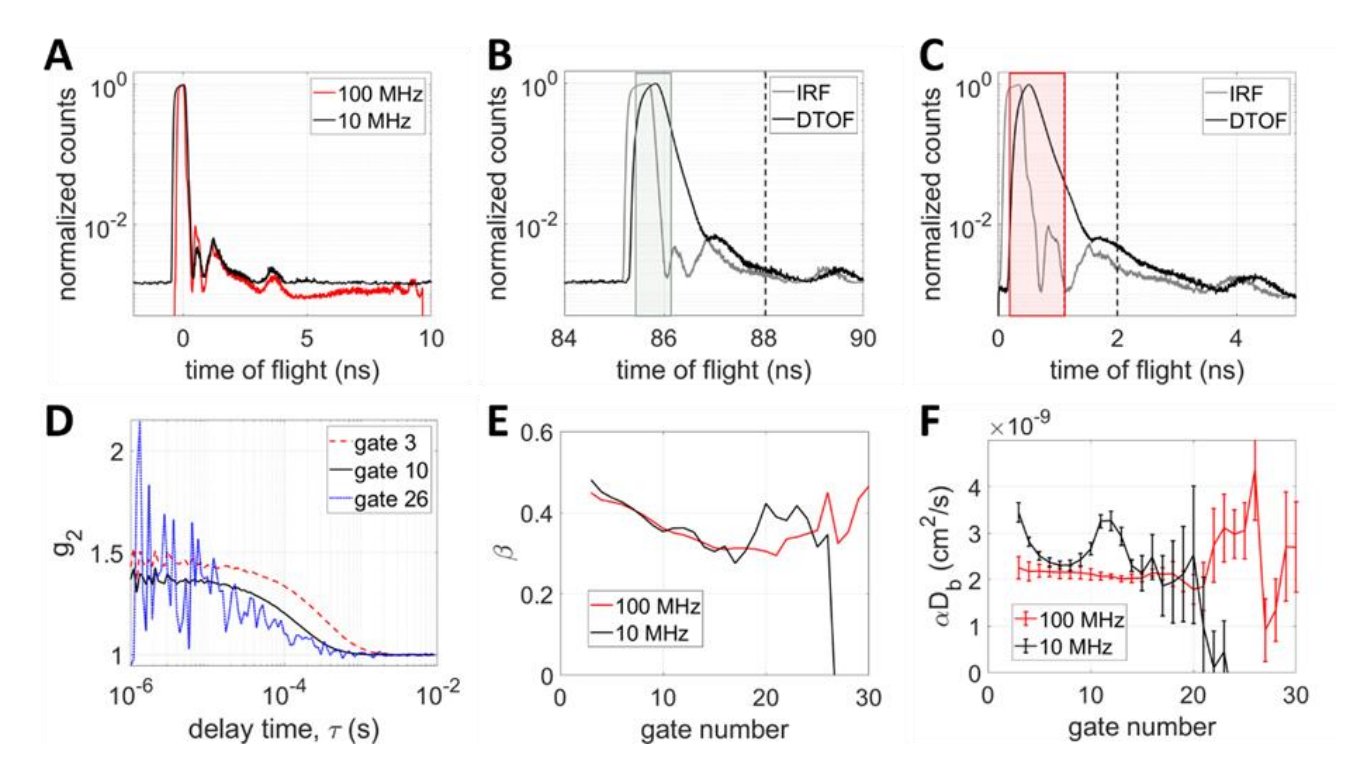


Figure 4. Results of time-gated analysis of DCS data. Two laser repetition rates were measured with slightly different IRF widths (subplot A). In subplots B and C, a zoom-in of the IRF together with the respective measured DTOFs are shown for the measurement at 10 MHz (subplot B) and the measurement at 100 MHz (subplot C). Values of (subplot E) were estimated from the time-gated g_2 curves (subplot D). Using these values of β , g_1 was calculated and finally αD_b was derived for all of the time-gates that were considered (subplot F). The time-gates were chosen so that their widths were approximately equal to the FWHM of the IRF, and each time-gate overlapped with 80% of the previous time-gate. The shaded regions in subplot B and C indicate the limits of the time gates which displayed relatively stable values of αD_b . The dashed vertical line in subplots B and C indicate the upper limit of the last considered time gate.

As can be observed in Figure 4, the measured DTOFs at 10 MHz and 100 MHz are shown in subplots B and C respectively. Note that the time-gates that were considered in this analysis are not shown individually. The values of β estimated from the time-gated g_2 curves (examples for data taken at 100 MHz are shown in subplot D) are plotted for each time-gate and both laser configurations in subplot E. For both laser configurations, in the earlier time-gates, β clearly decreases with later time-gates. At later time-gates, this trend in β is lost due to the noisy g_2 curves making it more difficult to estimate β . This is also reflected in the values of αD_b , where in particular for the data using 100 MHz, αD_b values are constant for time-gates up until approximately gate 15. After this gate, the values in



are noisier, and for the very late gates the values are no-longer constant. With the laser at 10 MHz, the range of time-gates for which αD_b was found to be constant was significantly narrower (approximately between gates 6 and 9). The portion of the DTOF curves that correspond to the gate limits where αD_b was found to be relatively stable is shown as the shaded region in subplots B and C. Furthermore, the limit of the end of the last gate considered (i.e. the last portion of the DTOF considered for time-gate analysis) is denoted by the dashed vertical lines in subplots B and C. The time-gated analysis fails at very late gates due most likely to the low detected photon-count rates but, in conclusion to this first analysis, the proposed laser appears to be appropriate for TD-DCS.

With these good results over the whole parameter space, we chose to operate at 100 MHz and 300 ps for the remaining experiments.

For the second experiment, to check for accuracy, the changing value of αD_b due to the increasing viscosity of the sample was plotted against the theoretical expectation as can be seen below.

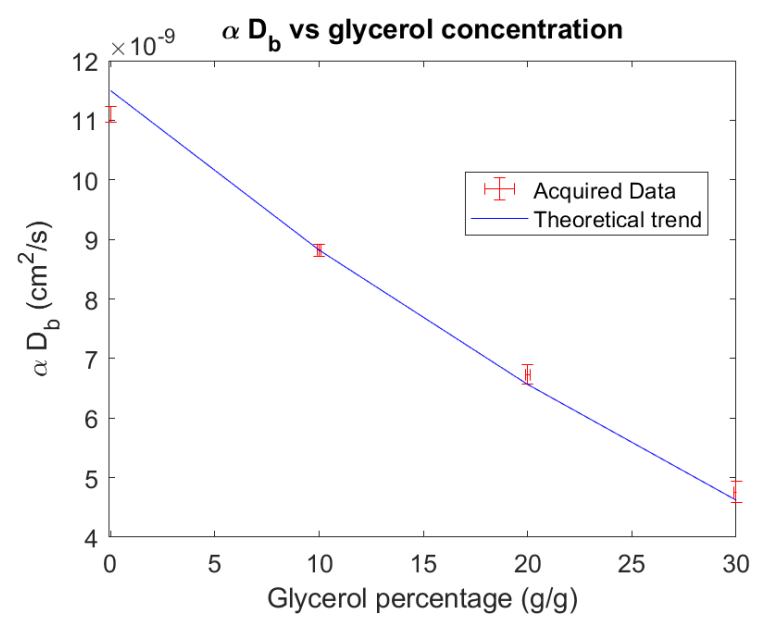


Figure 5. The measured value of α Db for liquid phantoms with varying concentrations of glycerol (as percentage of mass), but constant optical properties, plotted over the theoretical expectation based on experimental values of viscosity for water-glycerol mixtures and a theoretical model relating the viscosity of a liquid to its Db coefficient. This measurement was done with the laser set at 100 MHz and 300 ps pulse duration.

As can be seen from Figure 5, the acquired data reflects very well the expected theoretical trend, confirming that the 1064 nm laser operating at 100 MHz with a pulse with of 300 ps is satisfyingly accurate for this type of work.

For the third part of the experiment the final validation for TD-DCS was to carry out an in-vivo



measurement on a healthy volunteer. The arterial occlusion task shows change in the relative value of D_b over time as can be seen in the plot below.

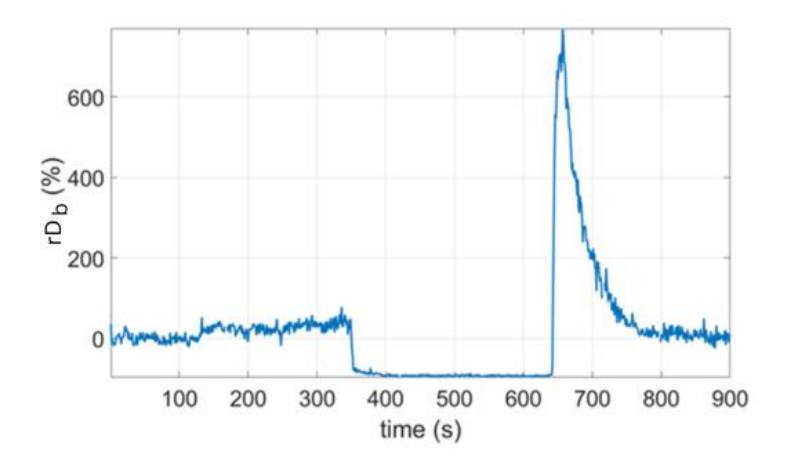


Figure 6. Relative change of the Db coefficient with respect to the baseline value for a task including: 350 s of rest, 300 s of arterial occlusion and 250 s of recovery. This measurement was done with the laser at 100 MHz and 300 ps pulse duration.

As can be seen from Figure 6, the behaviour of rD_b during and after the cuff occlusion is what we expect: an absence of moving blood during the occlusion followed by a surge in flow during the first moments of recovery; all is described by a value of rD_b of almost -100% during the 5 minutes of occlusion followed by a sharp increase of rD_b to more than +700% (relative to the baseline value).

3 Definition of the second wavelength for TD-NIRS

3.1 Problem

The other essential task of the multi-functional tomograph is to carry out TD-NIRS measurements. For this type of measurement, a minimum of two wavelengths is required to extract the HbO₂ and Hb concentrations. For standard NIRS applications it is common to use wavelengths like 690 nm and 830 nm. While it would be possible to construct a prototype with three laser sources (1064 nm for TD-DCS and the aforementioned two for TD-NIRS), it was of scientific interest and also practical convenience to investigate if TD-NIRS could be carried out with 1064 nm in combination with another wavelength. Indeed, understanding whether it's possible to carry out TD-NIRS with 1064 nm coupled to a second wavelength could lead to the decision to include only these two laser sources in the final prototype.



3.2 Methods and Setup

To evaluate whether 1064 nm can function as a good second wavelength for TD-NIRS, we carried out a cuff occlusion task on three healthy volunteers. The measurements got approved by the Ethical Committee of Politecnico di Milano and they were conducted in compliance with the Declaration of Helsinki.

The task comprised of:

- 1 minute of rest (baseline),
- 3 minutes of arterial occlusion at 200 mmHg,
- 4 minutes of recovery,
- 1 minute of venous occlusion at 100 mmHg,
- 2 minutes of recovery.

The laser source utilised was a supercontinuum pulsed laser (SuperK FIANIUM, NKT Photonics, Denmark). Its white light was injected into an acousto-optic filter (SuperK SELECT, NKT Photonics, Denmark) operated by a multi-input module (SuperK COMMAND, NKT Photonics, Denmark) which received electrical inputs from a GPIO (General Purpose Input/Output) (USB6229, National Instruments, USA). This complex setup was used to create pulses of light at 40 MHz which changed in wavelength at a rate of 800 Hz. It was set up to cycle through 8 different wavelengths chosen based on preliminary work with the setup. Those wavelengths were 690 nm, 750 nm, 785 nm, 800 nm, 830 nm, 860 nm, 900 nm and 1064 nm. With this setup a complete cycle of all the wavelengths done once was carried out every 10 ms.

The light originating from the acousto-optic filter was directed to a 1 mm core diameter fibre onto the skin of the healthy volunteers and held still with a probe and medical tape. The probe was placed on the most muscular part of the inside of the right forearm, assessed for each volunteer individually. The light was then collected with a fibre held 2 cm away from the injection fibre and directed to a detector (a homemade Silicon Photomultiplier module, as described in [6]). The detector sent its electronic signals to a data acquisition board (SPC-130, Becker and Hickl, Germany). The board also received a synchronization signal originating directly from the supercontinuum laser trigger signal.

To separate the data associated with each wavelength, the GPIO also controlled the data acquisition board by changing the acquisition channel at the same time as the wavelength was changed, guaranteeing that on each channel the data would be coming from only one wavelength (with <1%)



cross-talk for the process).

For the task-related setup, we wrapped a blood pressure cuff around the right bicep of each volunteer and inflated it manually following the task described above.

3.3 Analysis

To carry out a NIRS analysis we fitted all the DTOFs to obtain a value of μ_a (the absorption coefficient) for each curve. The model we used to describe the contribution of HbO₂ and Hb to absorption is the following:

$$\begin{split} &\mu_{a_{tot}}(\lambda_1) = \varepsilon_0(\lambda_1) \, \rho_0 + \, \varepsilon_H(\lambda_1) \, \rho_H + \mu_{a_{H_2O}}(\lambda_1) \\ &\mu_{a_{tot}}(\lambda_2) = \varepsilon_0(\lambda_2) \, \rho_0 + \, \varepsilon_H(\lambda_2) \, \rho_H + \mu_{a_{H_2O}}(\lambda_2) \end{split} \tag{eq. 4}$$

where $\mu_{a_{tot}}$ is the absorption coefficient extracted from the DTOF curves, ρ_0 is the concentration of HbO₂, ρ_H for Hb, ε_0 represents the specific absorption coefficient for HbO₂, ε_H for Hb and $\mu_{a_{H_20}}$ represents the contribution to absorption due to water in the biological tissue. From experimental data this can be approximated to be zero for all wavelengths between 690 and 900 nm, while for 1064 nm it is roughly 60% of the total absorption varying between 70% and 50% from subject to subject. The other absorbing substances are assumed to have a low enough contribution to the total absorption coefficient to be neglected in the calculation. With the water absorption correction and experimentally obtained values of the specific absorptions for all the wavelengths in this study, equation 6 reduces to a 2x2 matrix multiplying a vector of the concentrations of HbO₂ and Hb to obtain the total absorptions. We inverted the 2x2 matrix and operated it on the vector of the total absorptions to obtain the concentrations of the two types of haemoglobin. When carrying out this calculation we used 1064 nm for λ_1 and the other 7 wavelengths for λ_2 . We also carried out this calculation for a standard combination of wavelengths often used in NIRS: 690 and 830 nm.

For every combination of wavelengths we verified graphically the trend of the concentrations of the haemoglobins against the time during which we carried out the blood pressure task for all the patients. We calculated, for every combination of wavelengths, the condition number of the 2x2 matrix of specific absorption coefficients. Then, taking the average value of total absorption in the baseline part of the task where needed, we calculated the following quantities:

- the percentage error of the total concentration of haemoglobin, calculated as standard deviation divided by mean value of the concentration;
- 2. the concentration of HbO₂:

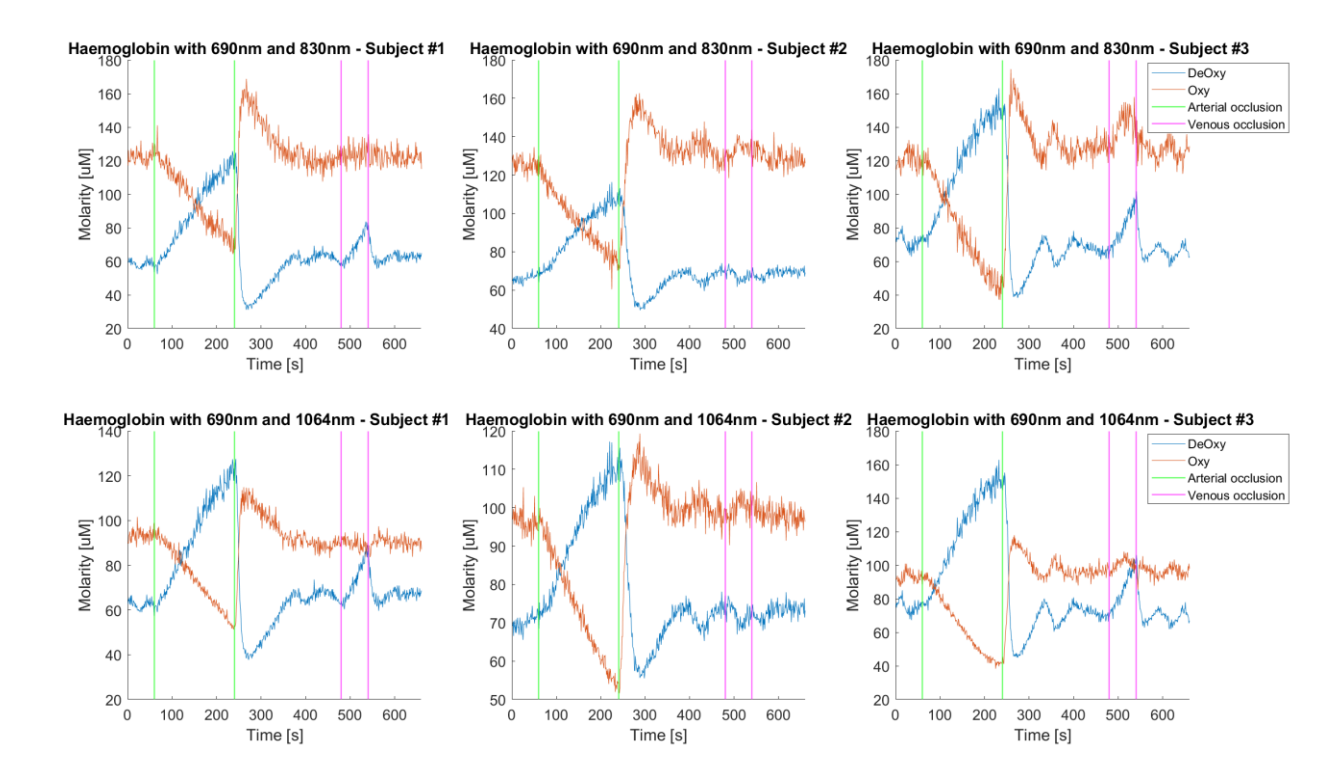


- the concentration of Hb;
- 4. the percentage saturation of haemoglobin;
- **5.** the total concentration of haemoglobin.

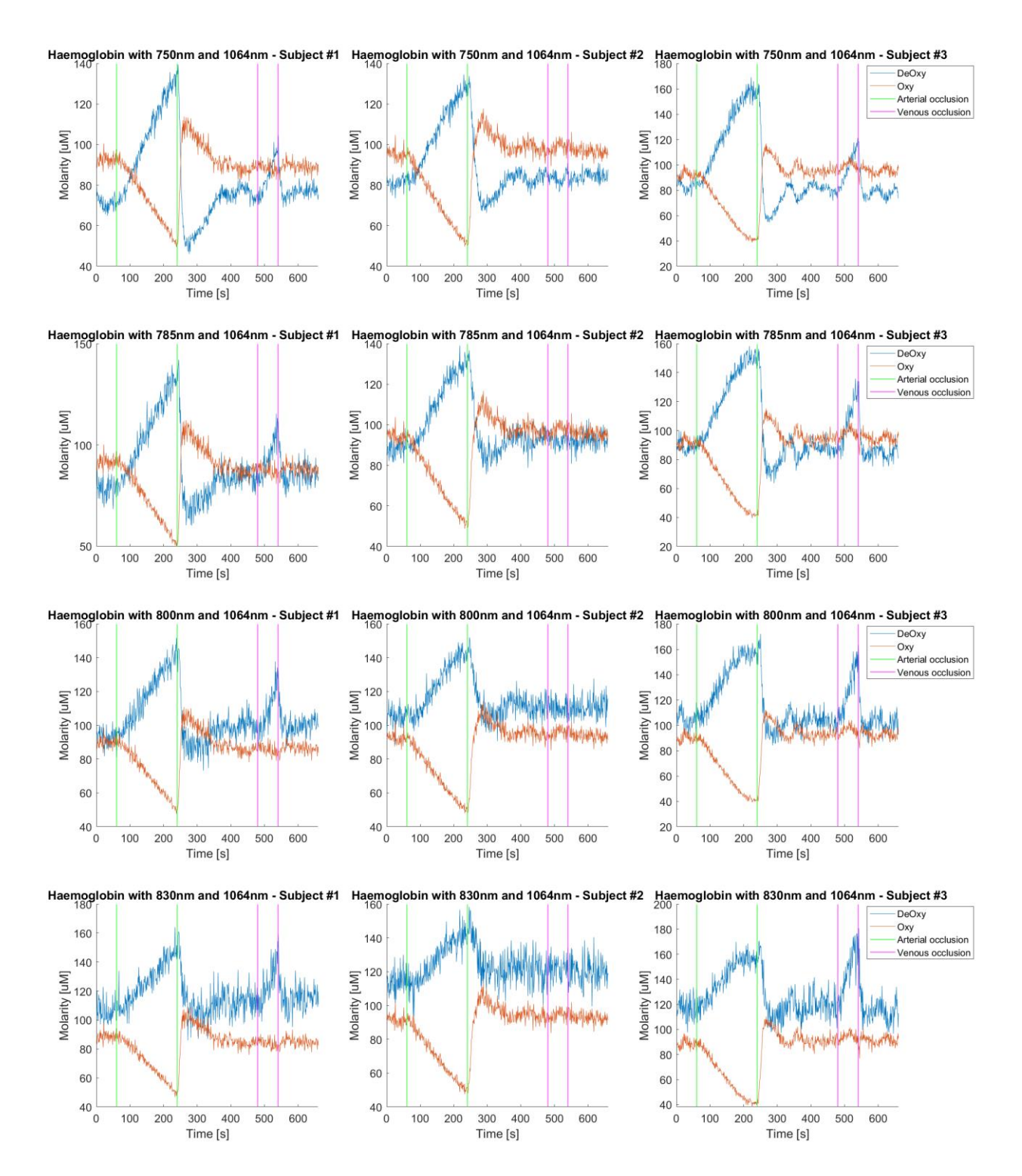
For the last four quantities (2-3-4-5), we also considered the uncertainty related to the water contribution to absorption. To do so, we repeated the calculations for water absorption contributions of 70% and 50% compared to the original calculations with 60%. We then evaluated a percentage error associated to each quantity \boldsymbol{A} as follows: $\%err = 100 \frac{|A_{70\%} - A_{50\%}|}{2A_{60\%}}$. We used this expression based on the assumption that the quantities change symmetrically around the value of $A_{60\%}$.

3.4 Results

In this experiment three healthy volunteers underwent a cuff-occlusion task with both arterial and venous occlusion. The evolution of the concentrations of HbO₂ and Hb is superimposed with the tasks and is shown in the plots below for different combinations of wavelengths.









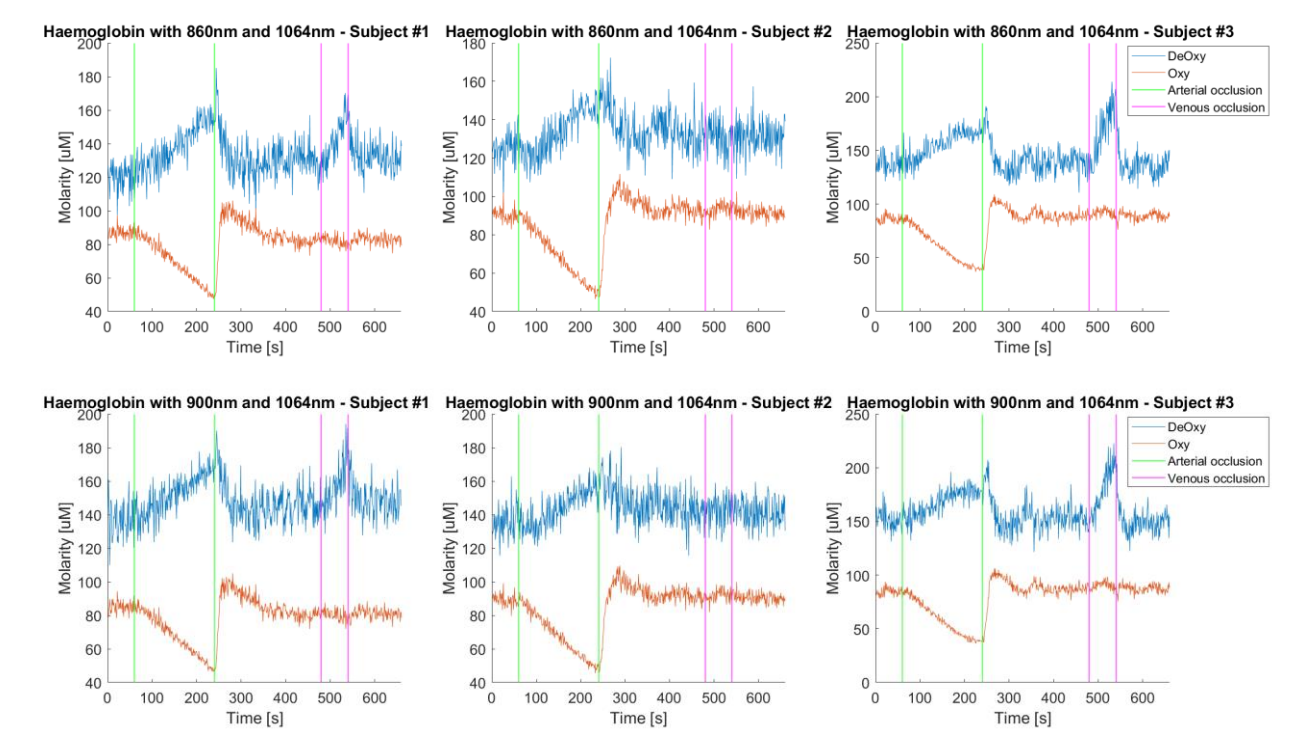


Figure 7. The measured values of HbO₂ and Hb in molarity for a task made of 1 min of rest, 3 min of arterial occlusion, 4 min of recovery, 1 min of venous occlusion, 2 min of recovery for various combinations of wavelengths (rows) and the three volunteers (columns).

As can be seen from Figure 7, the general trend is that HbO₂ decreases during the arterial occlusion but remains constant during the venous occlusion as expected. For Hb the inverse is true during the arterial occlusion, and it increases during the venous occlusion as expected. This isn't noticeable for Subject #2, possibly due to an incomplete venous occlusion (e.g., not inflating the cuff to a high enough pressure for the venous occlusion to take place). Another detail can be seen from Figure 7 is that the curves look less noisy for the gold standard NIRS combination (690 nm and 830 nm) and for the 690-1064 combination while the curves look noisier for the combinations of 1064 nm and wavelengths longer than 800 nm. This is due, in part to the condition number of the matrix of specific absorption for each wavelength combination, as can be seen in the plots below.



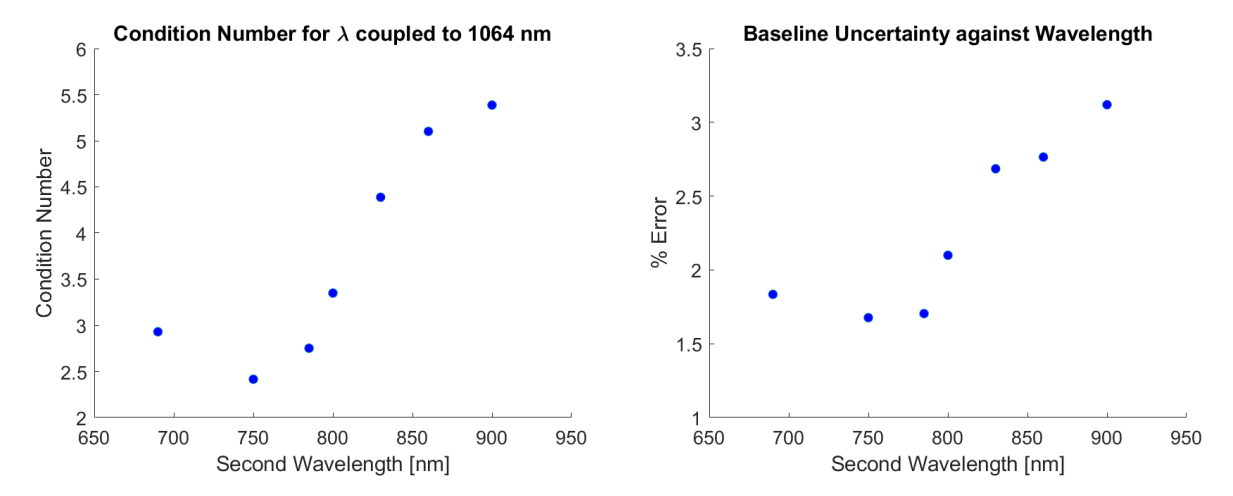
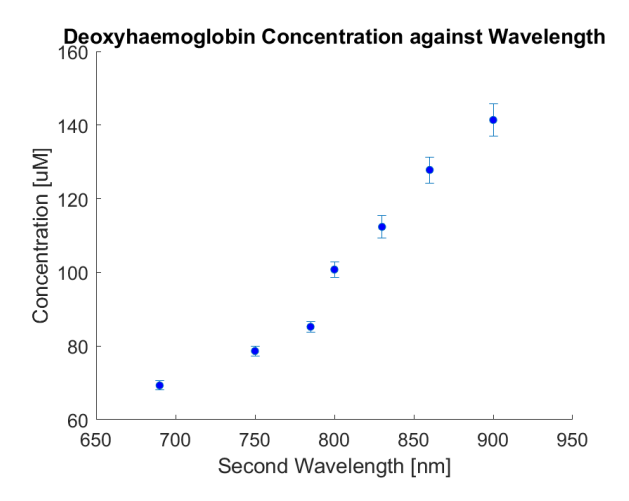
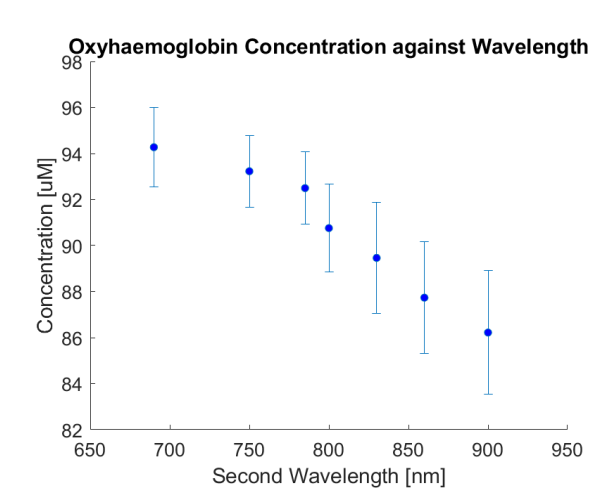


Figure 8. Left: the condition number of the matrix of specific absorptions plotted against the wavelength coupled to 1064 nm and Right: the percentage uncertainty of the measured baseline values of the total haemoglobin concentration (averaged over the three volunteers) plotted against the wavelength coupled to 1064 nm.

As can be seen in Figure 8, the baseline uncertainty error increases with the second wavelength coupled to 1064 nm, the error is also shown to increase with the condition number. This initially suggests it is best to operate with a smaller second wavelength, further analysis on the effect of the wavelength choice is shown in the plots below.







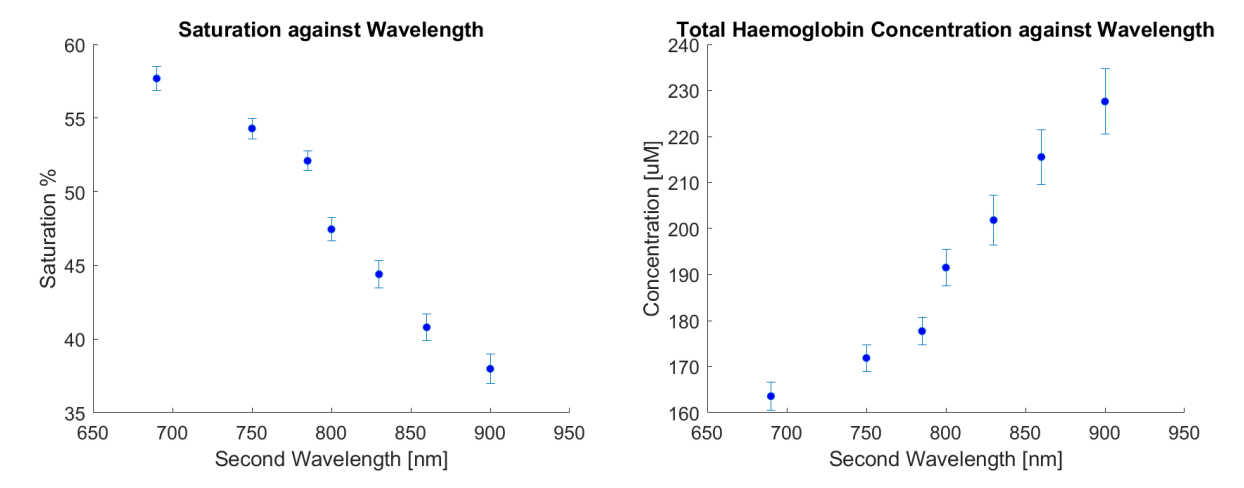
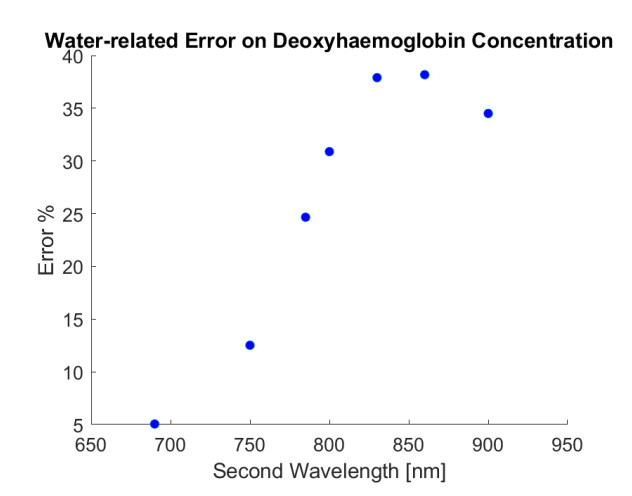
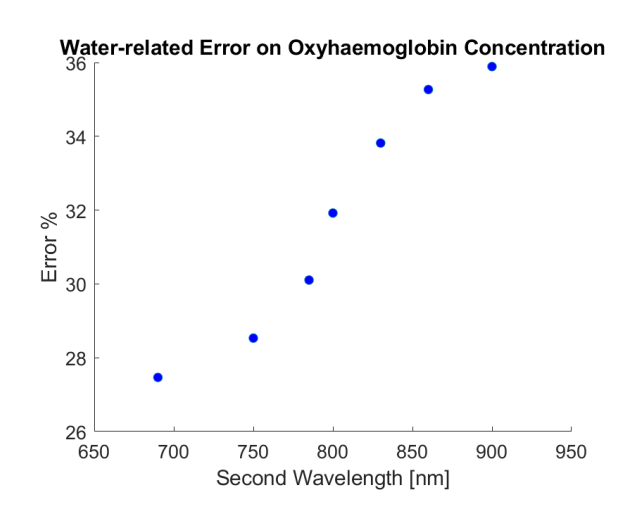


Figure 9. Haemoglobin related quantities evaluated at each second wavelength (the wavelength coupled to 1064 nm) for the baseline of the cuff occlusions. The average of the three volunteers was taken, and the error bars were evaluated using the baseline uncertainty shown in Figure 8. The quantities are, going from top left to bottom right: concentration of Hb as molarity, concentration of HbO₂, saturation of the blood, total haemoglobin concentration.

As can be seen in Figure 9, the baseline values of HbO₂ and Hb concentration, of saturation and of total haemoglobin concentration depends on the wavelength combination choice. The significant variation in these values (which doesn't reflect real differences in the sample composition), could be ascribed to the way the other chromophores contribution not enlightened in the analysis (e.g., lipids). In the first analysis we assumed a neglectable water absorption at all the second wavelengths and a 60% water absorption at 1064 nm. Water concentration might vary from subject to subject, so we evaluated the dependence of these quantities on the uncertainty of the water absorption percentage as can be seen in the plots below.







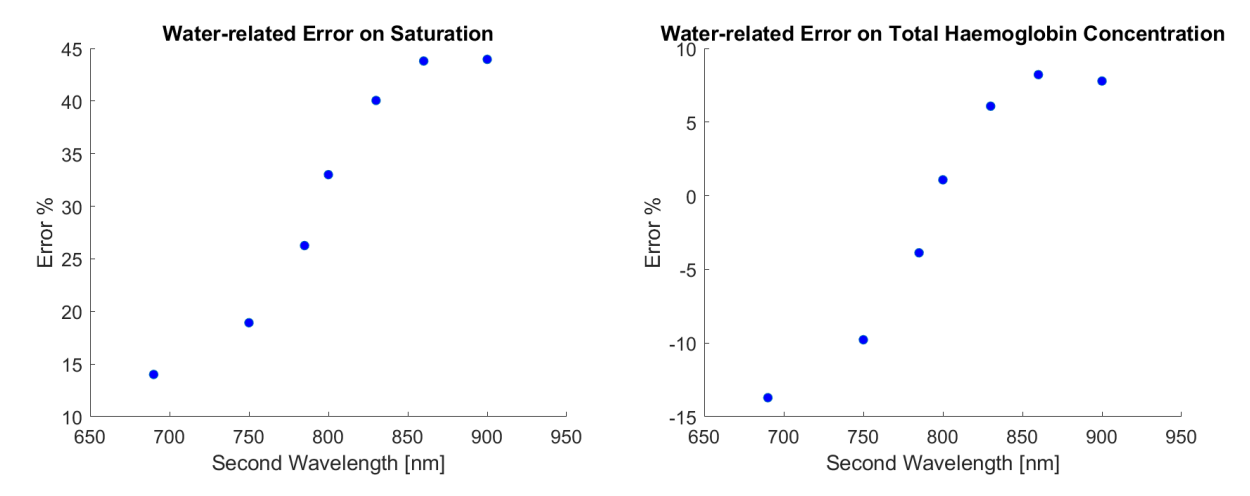


Figure 10. The error (on haemoglobin related quantities) associated to the uncertainty in the water absorption of the biological sample analysed. This error is evaluated for four quantities, going from top left to bottom right: concentration of Hb, concentration of HbO₂, saturation of the blood, total haemoglobin concentration. The errors are plotted against the second wavelength (the wavelength coupled to 1064 nm).

As can be seen in Figure 10, the error arising due to the imprecise percentage of water in the studied sample is unfortunately quite high, even for the lowest second wavelength.

4 Conclusion

We conclude that for TD-DCS the 1064 nm laser based on temporal slicing of a highly temporally coherent CW source is a suitable choice. The value of β for all parameter combinations is high when time-gates of comparable duration to the pulse is applied, meaning the pulse duration can be tuned slightly to accommodate for the depth selectivity of interest for the biological tissue being studied. The instability error is lower than 11% and doesn't depend much on the repetition rate and, similarly, the power output of the laser remains roughly constant when changing the repetition rate, allowing us to work with lower frequencies to reject environmental light noise. The laser itself finally is a compact device, and it's already close to being medical grade equipment as it is used for dermatological applications, meaning it's a good candidate for the fastMOT prototype.

For TD-NIRS, we confirmed that the same 1064 nm wavelength adopted for TD-DCS can be useful to retrieve information on HbO₂, given the low contribution of Hb at that wavelength [2]. Yet, a second wavelength possibly in the region <800 nm (the isosbestic point for Hb and HbO₂) is also needed to resolve Hb and therefore retrieve both the total haemoglobin content and the tissue oxygenation. Yet, the relevant contribution of water absorption at 1064 nm can affect the absolute estimate of HbO₂ content, causing a indeterminacy in the absolute value of HbO₂ due to the uncertainty in the



water content in tissues. A third wavelength to resolve also water content might be considered at the expenses of higher system complexity. Nevertheless, it must be noted that in most clinical cases a limited uncertainty in the baseline level of Hb and HbO₂ is acceptable provided that the relative temporal evolution of both components is properly tracked as confirmed with the in vivo tests on healthy volunteers.

5 References

- [1] L. Cortese et al., "Recipes for diffuse correlation spectroscopy instrument design using commonly utilized hardware based on targets for signal-to-noise ratio and precision", Biomed. Opt. Express 12, 3265-3281. (2021)
- [2] L. Di Sieno et al., "Oxyhemoglobin Measurements Using 1064 nm Light", in IEEE Journal of Selected Topics in Quantum Electronics, vol. 31, no. 4: Adv. in Neurophoton. (2024)
- [3] L. Colombo, "Time-domain diffuse correlation spectroscopy: from physics to biomedical applications". (2021)
- [4] L. K. Frisk et al., "fastMOT Deliverable 5.1". (2024)
- [5] Glycerine Producers' Association, "Physical properties of glycerine and its solutions", Glycerine Producers' Association. (1963)
- [6] D. Martinenghi et al., "Time-resolved single-photon detection module based on silicon photomultiplier: A novel building block for time-correlated measurement systems", Review of Scientific Instruments, 87(7). (2016)